Theory of edge-state optical absorption in two-dimensional transition metal dichalcogenide flakes

Maxim Trushin
Department of Physics, University of Konstanz, D-78457 Konstanz, Germany

Edmund J. R. Kelleher
Department of Physics, Imperial College London, London SW7 2AZ, England, United Kingdom

Tawfique Hasan
Cambridge Graphene Centre, University of Cambridge, Cambridge CB3 0FA, England, United Kingdom
(Received 19 February 2016; revised manuscript received 8 July 2016; published 6 October 2016)

We develop an analytical model to describe sub-band-gap optical absorption in two-dimensional semiconducting transition metal dichalcogenide (s-TMD) nanoflakes. The material system represents an array of few-layer molybdenum disulfide crystals, randomly orientated in a polymer matrix. We propose that optical absorption involves direct transitions between electronic edge states and bulk bands, depends strongly on the carrier population, and is saturable with sufficient fluence. For excitation energies above half the band gap, the excess energy is absorbed by the edge-state electrons, elevating their effective temperature. Our analytical expressions for the linear and nonlinear absorption could prove useful tools in the design of practical photonic devices based on s-TMDs.

DOI: 10.1103/PhysRevB.94.155301

I. INTRODUCTION

In the last decade, following the discovery of graphene [1], research of two-dimensional (2D) materials has experienced an explosive growth. A 2D material represents an atomically thin solid flake, with optical properties qualitatively different from its three-dimensional parent crystal [2,3]. One of the largest families of 2D materials is that of the transition-metal dichalcogenides (TMDs) that contains over 40 different forms, either metallic or semiconducting [2]. TMDs have the general formula MX_2, where M represents a transition metal, (e.g., molybdenum or tungsten) and X represents a chalcogen (e.g., sulfur, selenium, or tellurium) [2,3]. Single-layer MX_2 crystals are quasi-2D structures, containing a plane of metal (M) atoms covalently bonded between two planes of chalcogen (X) atoms; see Fig. 1(a). In contrast to bulk semiconducting TMD (s-TMD) crystals, their monolayers typically exhibit a direct band gap at visible or near-infrared frequencies, making them a suitable material for a range of photonic and optoelectronic applications [2,4–6]. In a direct band-gap semiconductor, with a pristine lattice and of infinite extent, photons with energies lower than the band gap cannot excite direct interband transitions; thus, single-photon absorption at these energies does not occur. Recent experiments by several research groups, however, have demonstrated both non-negligible linear absorption at sub-band-gap photon energies as well as a finite nonlinear optical response in a variety of s-TMDs, including MoS_2 [7,8], WS_2 [9,10], and $MoSe_2$ [11,12]. Liquid phase exfoliated $MoSe_2$-polymer composites, for example, have been reported to exhibit $>7\%$ linear absorption in the 0.65–0.8-eV range [11], in spite of $MoSe_2$ having a direct (in monolayer form) and indirect (bulk) band gap of $\sim$1.5–1.58 and $\sim$1.1 eV, respectively [3,13].

Several mechanisms have been proposed to explain this phenomenon. Supported by first-principles calculations, Wang *et al.* suggested that a reduction in the MoS_2 band gap could be achieved by introducing crystallographic defect states [14]. The authors also suggested that defects could activate the material as a broadband saturable absorber [14]. We recently proposed that edge states contribute to sub-band-gap absorption in s-TMDs [15,16]. This mechanism is supported by earlier photothermal deflection spectroscopy of MoS_2 nanoflakes, where increased linear absorption at sub-band-gap energies was observed for large MoS_2 crystals after lithographic texturing that increased the total amount of edges in the sample [17]. The s-TMD flakes prepared by liquid phase exfoliation (LPE)—a widely used technique for the low-cost, mass manufacture of nanomaterials—also have a high edge to surface area ratio, and are thus expected to exhibit sub-band-gap states, supporting absorption of photons with lower energies than the material band gap. Recent studies have demonstrated that the sub-band-gap absorption in s-TMD nanoflakes can be saturated, and exploited this effect in the development of ultrafast lasers operating in near infrared, corresponding to photon energies in the range 0.6–1.12 eV [7–12,15]. While a growing body of experimental work continues to substantiate the process of sub-band-gap absorption in s-TMDs, and practical applications of this phenomenon are being leveraged in the field of photonics, theoretical analyses are limited and the origin of sub-band-gap optical absorption remains an open question. Here, we develop an analytical theory, testing the hypothesis of edge-mediated absorption in s-TMDs to explain the phenomenon of sub-band-gap saturable absorption.

The electronic states at the edges of a nanoflake (edge states) have been modeled to date using two approaches: first, by focusing on the atomic structure of a particular edge and computing the energy dispersion by means of a tight-binding Hamiltonian with appropriate boundary conditions [19–23]; second, using density functional theory [24–30]. It has been shown a few years ago [31] that the chalcogen-terminated zig-zag edges are the most stable because they have lowest energies without hydrogen saturation. We therefore expect such edge types to be the most abundant in the dispersion of

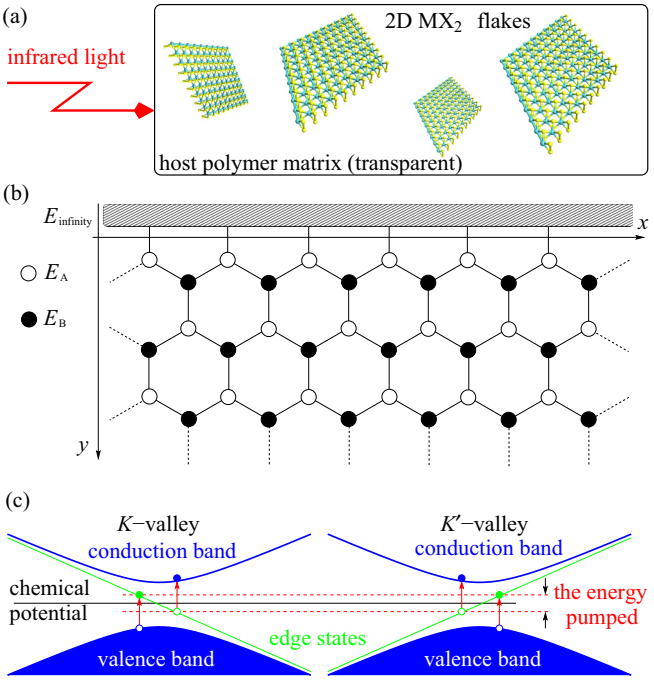

FIG. 1. (a) The s-TMD flakes are randomly distributed within a host polymer matrix illuminated by infrared light with an excitation energy below the material band gap. (b) The honeycomb lattice with the on-site energies E_A and E_B terminated by the barrier along the x axis, where E_B becomes infinite. (c) The electronic band structure of a single flake includes conduction, valence, and edge states. The edge states are one-dimensional, i.e., the depicted momentum axis is parallel to the flake's edge. There are two mirror copies of these bands in the first Brillouin zone (K and K' valley). For a given excitation energy, two *independent* optical absorption channels are possible in each valley corresponding to the valence-to-edge and edge-to-conduction bands direct transitions. These transitions are shown by red arrows, and the electrons and holes created are depicted by the filled and empty circles, respectively; see also Fig. 6 in Ref. [18]. Each edge-state electron-hole pair accumulates a certain amount of energy which after thermalization appears as an elevated temperature for the edge-state electrons.

nonhydrogenated 2D TMDs. Moreover, such edges maintain one-dimensional (1D) metallic states, as confirmed by *ab initio* [26,30] and continuum-model [18] calculations. The latter shows that the band structure of the purely dichalcogen-terminated zig-zag edge can be well approximated by 1D bands with linear dispersions, where electrons are propagating in opposite directions in the K and K' valleys. Our model shown in Figs. 1(b) and 1(c) mimics this behavior, but, in contrast to the previous approaches, allows us to calculate the wave functions and the Fermi's golden-rule optical transitions from and to the edge states analytically. In detail, we use an effective Hamiltonian proposed in Ref. [32] but with a spatially dependent band gap simulating the flake edge. A somewhat similar model is known in the literature as a neutrino billiard [33].

The *ab initio* calculations reviewed above are able to provide a quantitative description of the optical absorption of a particular flake with a given edge type; however, experimental measurements are typically preformed on an array of small flakes, randomly oriented in a polymer, with different edge types. We therefore need an effective model which focuses on the most optically active metallic states supported by the most stable chalcogen-terminated zig-zag edges. The model may not be valid for isolated flakes that may not possess metallic edge states. Nonetheless, it should provide a reliable optical absorption estimate for a large ensemble of flakes, where optically inert edge states are dominated by their active counterparts. Focusing on the most important edge type allows for explicit expressions for the linear and saturable optical absorptions. The compromise for this simplification is the lack of predictive power on the quantitative level.

The peculiarities of the edge-state absorption are depicted in Fig. 1. In contrast to the two-band model for bulk semiconductors [34], our approach involves *three* electron subsystems. A one-dimensional edge-state electron subsystem always remains in the metallic regime with the Fermi energy determined by the bulk chemical potential. In contrast, the conduction and valence bands are in the semiconducting regime: the valence band is occupied almost completely whereas the conduction band is nearly empty. Subgap direct transitions occur between the valence-band and edge states as well as the edge and conduction-band states. The relative contribution of these two transitions is determined by Pauli blocking and depends on the relationship between the excitation frequency and the Fermi level. We show that despite the complexity of the model the saturable subgap absorption A^Φ for s-TMD flakes can be written in the conventional form [34]

$$A^\Phi = \frac{A}{1+\frac{\Phi}{\Phi^s}}, \tag{1}$$

where A is the relative linear absorption estimated by Eq. (17), Φ is the incident fluence, and Φ^s is the saturation fluence given by Eq. (24). The absorption is defined as a ratio of the absorbed radiation fluence to the incident fluence. In the rest of the paper, we derive the analytical expressions for A and Φ^s, and analyze their behavior.

II. MODEL

From the point of view of the band theory, the difference between semiconductor and vacuum can be described by means of the band gap Δ: it is finite in the semiconducting region but infinite outside, where no conduction is possible. Let us consider a simple Hamiltonian derived for electrons on a honeycomb lattice using the tight-binding approach with the lattice constant a, the on-site energies $E_{A,B}$, and the nearest-neighbor hopping $t_\perp$. Near the K corner of the hexagonal first Brillouin zone, the Hamiltonian can be written in the continuum limit as [35]

$$H_0^K = \begin{pmatrix} E_A & -t_\perp \frac{\sqrt{3}a}{2}(\hat{k}_x - i\hat{k}_y) \\ -t_\perp \frac{\sqrt{3}a}{2}(\hat{k}_x + i\hat{k}_y) & E_B \end{pmatrix},$$

where $\hat{k}_x = -i\partial_x$, $\hat{k}_y = -i\partial_y$ are momentum operators. (The Hamiltonian for the K' corner can be obtained by the substitution $\hat{k}_x \to -\hat{k}_x$.) This Hamiltonian can be rewritten in a more instructive form given by [32]

$$H_0^K = \text{const} + \begin{pmatrix} \frac{\Delta}{2} & \hbar v(\hat{k}_x - i\hat{k}_y) \\ \hbar v(\hat{k}_x + i\hat{k}_y) & -\frac{\Delta}{2} \end{pmatrix}, \tag{2}$$

where const $= (E_A + E_B)/2$, $\Delta = E_A - E_B$ represents the band gap, and $-\sqrt{3}at_\perp/2 = \hbar v$, with $\hbar v = 1.1$ eV $\times$ 3.193 Å for MoS_2 [32]. The gap can be either positive or negative depending on the difference between the on-site energies $E_{A,B}$. The spin-orbit coupling is neglected here. It results in the valley-spin locking which, in turn, can be used for the valley-selective pump-probe spectroscopy with circularly polarized light. Since we are dealing with the linear polarization, both valleys contribute equally and the only effect of the spin-orbit splitting is the spin-dependent band gap.

The edge states along the x axis can be simulated by means of a y-dependent gap $\Delta(y)$. We first solve the edge-state spectral problem for K-valley $H_0^K \psi_e = E_e \psi_e$ and obtain the eigenstate wave function ψ_e in the form

$$\psi_e = C \exp\left(ik_x x - \int_0^y \frac{\Delta(y')dy'}{2\hbar v}\right)\begin{pmatrix}1\\-1\end{pmatrix}, \tag{3}$$

where C is a normalization constant, and $\Delta(y)$ should change its sign at $y = 0$ [36]. An edge along the y axis can be modeled in a similar way by an x-dependent gap $\Delta(x)$. Since we aim for an analytical derivation of the linear absorption and saturation fluence, we simplify $\Delta(y)$ as

$$\Delta(y) = \begin{cases}\Delta > 0, & y \geqslant 0 \quad \text{(semiconductor)}\\ -\infty, & y < 0 \quad \text{(vacuum)}\end{cases}. \tag{4}$$

Equation (3) then reads

$$\psi_e = \sqrt{\frac{\Delta}{2L\hbar v}} \exp\left(ik_x x - \frac{y\Delta}{2\hbar v}\right)\begin{pmatrix}1\\-1\end{pmatrix}, \quad y \geqslant 0, \tag{5}$$

which is normalized as

$$\lim_{W\to\infty} \int_0^L dx \int_0^W dy(\psi_e^\dagger \psi_e) = 1$$

and obeys the dispersion $E_e = -\hbar v k_x$. Due to Eq. (4), ψ_e exponentially vanishes in the bulk because $\Delta > 0$ at $y \geqslant 0$. Note that ψ_e equals to zero at $y < 0$ but is finite at $y = 0$, i.e., it demonstrates a steplike behavior. This is because $\Delta(y)$ is not a true electrostatic potential, as emphasized by Berry and Mondragon [33], but a "staggered" one [20]. The staggered potential depends on the sublattice, whereas true electrostatic potential does not. Even if $\Delta(y)$ goes to infinity, it is not equivalent to the hard-wall potential, where the wave function must vanish at the border. For the K' valley, the solution of the spectral problem results in the same dispersion E_e but taken with an opposite sign; see Fig. 1(c). In contrast to a topological quantum-Hall insulator [36], the edge states (5) exist in two mirror copies in two valleys. To give an example, the edge-state electrons in MX_2 monolayers may experience intervalley backscattering, i.e., the edge-state electron transport is not topologically protected. It is worth emphasizing that our conclusions do not depend on whether the edge is along the x or y direction since the optical absorption is averaged over the flake orientation.

The bulk conduction-band eigenwave functions for the K valley are given by

$$\psi_c = \frac{1}{\sqrt{LW}} \exp(ik_x x + ik_y y)\begin{pmatrix}\cos\frac{\theta}{2}\\ \sin\frac{\theta}{2}e^{i\phi}\end{pmatrix}, \tag{6}$$

with the dispersion $E_c = \sqrt{(\hbar v k)^2 + \Delta^2/4}$, whereas the valence-band wave functions read

$$\psi_v = \frac{1}{\sqrt{LW}} \exp(ik_x x + ik_y y)\begin{pmatrix}\sin\frac{\theta}{2}\\ -\cos\frac{\theta}{2}e^{i\phi}\end{pmatrix}, \tag{7}$$

with the dispersion $E_v = -\sqrt{(\hbar v k)^2 + \Delta^2/4}$. Here,

$$\tan\theta = \frac{2\hbar v k}{\Delta}, \quad \tan\phi = \frac{k_y}{k_x}.$$

The bulk states are normalized to unity on the rectangle $0 \leqslant x \leqslant L, 0 \leqslant y \leqslant W$.

The electron-photon interaction Hamiltonian for the K valley is derived from Eq. (2) and is given by [37,38]

$$H^{\text{int}} = \frac{evE_0}{2\omega}\begin{pmatrix}0 & e^{-i\theta_E}\\ e^{i\theta_E} & 0\end{pmatrix},$$

where E_0, ω, and θ_E are the electromagnetic wave amplitude, frequency, and polarization angle correspondingly. The valence-to-edge states transitions are described by the following matrix element:

$$\begin{aligned}\langle\psi_e|H^{\text{int}}|\psi_v\rangle = &-\sqrt{\frac{\Delta}{2\hbar W v}}\frac{evE_0}{2L\omega}\\ &\times\left(\cos\frac{\theta}{2}e^{i\phi-i\theta_E} + \sin\frac{\theta}{2}e^{i\theta_E}\right)\\ &\times\frac{e^{i(k_x-k_x')L}-1}{i(k_x-k_x')}\frac{e^{(ik_y-\frac{\Delta}{2\hbar v})W}-1}{ik_y-\frac{\Delta}{2\hbar v}}.\end{aligned} \tag{8}$$

Here, $(k_x, k_y) = \mathbf{k}$ and k_x' are momenta components in the bulk and at the edge, respectively. The valence-to-edge states transition rate can be calculated as

$$\begin{aligned}g_{ev}^{\text{ph}}(\omega) = &\sum_{k_x,k_y,k_x'}\frac{2\pi}{\hbar}\left|H_{ev}^{\text{int}}\right|^2\left(f_v^{(0)} - f_e^{(0)}\right)\\ &\times\delta[-\hbar v k_x' + \sqrt{(\hbar v k)^2 + \Delta^2/4} - \hbar\omega],\end{aligned} \tag{9}$$

where $f_v^{(0)}$ and $f_e^{(0)}$ are the Fermi-Dirac distributions for electrons in the valence band and in the edge states, respectively and $|H_{ev}^{\text{int}}|^2$ reads

$$\begin{aligned}\left|H_{ev}^{\text{int}}\right|^2 &= \lim_{L,W\to\infty}|\langle\psi_e|H^{\text{int}}|\psi_v\rangle|^2\\ &= \frac{\Delta}{2\hbar v}\frac{2\pi}{LW}\delta(k_x - k_x')\left(\frac{evE_0}{2\omega}\right)^2\\ &\times\frac{1+\sin\theta\cos(\phi-2\theta_E)}{\left(\frac{\Delta}{2\hbar v}\right)^2 + k_y^2}.\end{aligned}$$

The edge-to-conduction-band transition rate differs from Eq. (9) by the sign in front of the θ_E-dependent term and by the filling factors. The corresponding generation rate reads

$$\begin{aligned}g_{ce}^{\text{ph}}(\omega) = &\sum_{k_x,k_y,k_x'}\frac{2\pi}{\hbar}\left|H_{ce}^{\text{int}}\right|^2\\ &\times\delta[\sqrt{(\hbar v k)^2 + \Delta^2/4} + \hbar v k_x' - \hbar\omega]\left(f_e^{(0)} - f_c^{(0)}\right),\end{aligned} \tag{10}$$

where

$$\left|H_{ce}^{\rm int}\right|^2 = \lim_{L,W\to\infty} |\langle\psi_c|H^{\rm int}|\psi_e\rangle|^2 = \frac{\Delta}{2\hbar v}\frac{2\pi}{LW}\delta(k_x - k_x')\left(\frac{evE_0}{2\omega}\right)^2 \times \frac{1-\sin\theta\cos(\phi-2\theta_E)}{\left(\frac{\Delta}{2\hbar v}\right)^2 + k_y^2},$$

and $f_c^{(0)}$ stands for the conduction-band Fermi-Dirac distribution.

The flakes are randomly oriented, thus the relative optical absorption is determined by the ratio between the θ_E-averaged absorbed power $\hbar\omega\langle g_{ev}^{\rm ph} + g_{ce}^{\rm ph}\rangle_{\theta_E}$ and the incident radiation power $(cE_0^2 S)/(8\pi)$ with S being the illuminated area. To sum up over k_x', k_x, and k_y we transform sums to integrals as

$$\sum_{k_x,k_y,k_x'} \to \int \frac{dk_x' L}{2\pi}\int\frac{dk_x L}{2\pi}\int\frac{dk_y W}{2\pi}.$$

The integral over k_x' is taken using the momentum conservation represented above as $\delta(k_x - k_x')$. The integral over k_x is then taken using the energy conservation utilizing the transformation

$$\delta\left(\sqrt{(\hbar vk)^2 + \Delta^2/4} \pm \hbar vk_x - \hbar\omega\right) = \frac{\hbar^2\omega^2 + \Delta^2/4 + \hbar^2v^2k_y^2}{2\hbar^3\omega^2 v} \times \delta\left(k_x \mp \frac{\hbar^2\omega^2 - \Delta^2/4 - \hbar^2v^2k_y^2}{2\hbar^2\omega v}\right).$$

We then substitute $\hbar vk_y = \varepsilon$, $E_\omega = \hbar\omega$ and obtain the relative absorption of a single edge A_1 in the form $A_1 = A_1^+ + A_1^-$, where $A_1^\pm$ correspond to the $v \to e$ and $e \to c$ transitions, respectively, and are given by

$$A_1^\pm = \frac{e^2}{\hbar c}\frac{\hbar vL}{S}\frac{\Delta}{4E_\omega}\int_{-\infty}^{\infty} d\varepsilon\left(\frac{1}{E_\omega^2} + \frac{1}{\varepsilon^2 + \Delta^2/4}\right)F^\pm(\varepsilon). \tag{11}$$

Here, $F^\pm(\varepsilon)$ describe the corresponding occupations and are given by

$$F^+(\varepsilon) = \frac{1}{1+\exp\left(-\frac{\varepsilon^2+\Delta^2/4+E_\omega^2}{2E_\omega T_0} - \frac{\mu_p}{T_0}\right)} - \frac{1}{1+\exp\left(-\frac{\varepsilon^2+\Delta^2/4-E_\omega^2}{2E_\omega T} - \frac{\mu}{T}\right)}, \tag{12}$$

$$F^-(\varepsilon) = \frac{1}{1+\exp\left(\frac{\varepsilon^2+\Delta^2/4-E_\omega^2}{2E_\omega T} - \frac{\mu}{T}\right)} - \frac{1}{1+\exp\left(\frac{\varepsilon^2+\Delta^2/4+E_\omega^2}{2E_\omega T_0} - \frac{\mu_n}{T_0}\right)}. \tag{13}$$

Here, we set different (fluence dependent) quasi Fermi levels [39] μ_n and μ_p for the conduction and valence bands correspondingly. The quasi Fermi levels μ_n and μ_p are both equal to the equilibrium chemical potential μ as long as no interband transitions occur and no photocarriers are excited. These notations will be utilized in Sec. IV devoted to the saturable absorption. Moreover, two temperatures have been introduced: T_0 is the lattice temperature for bulk electrons, and T is the temperature for edge-state electrons which may differ from T_0 in some cases described in Sec. V.

We emphasize that Eq. (11) describes the optical absorption of a *single* edge of a *single* flake for a *given* spin and valley channel. The total absorption of a s-TMD dispersion or a s-TMD-polymer composite should take into account different spin and valley channels as well as the concentration of flakes. It can be shown that the K'-valley edge states result in the same contribution to the absorption as Eq. (11). The spin-split absorption channels give two different contributions determined by the spin-dependent band-gap value $\Delta = \Delta_s$, but we neglect the spin splitting for the sake of simplicity. Moreover, we assume that the flakes are squares of the size d, and all flakes are placed perpendicular to the light beam. To sum up these contributions, we define an *effective* length as

$$L^{\rm eff} = \ell S \quad \text{with} \quad \ell = 4dg_{sv}n_{\rm 2D}, \tag{14}$$

where $4d$ is the average perimeter of a flake, $g_{sv} = 4$ is the spin/valley degeneracy, and $n_{\rm 2D}$ is the number of monolayer flakes per unit area of a composite film. The quantity ℓ then plays a role of the total effective length of monolayer flakes' edges per unit area of a composite film. Assuming the size of the flake to be of the order of 100 nm, the monolayer flake concentration $n_{\rm 2D} \sim 10^{11}$ cm^{-2}, we estimate the effective length to be of the order of 1 km for a 1 mm^2 spot size. In order to convert the absorption of a single edge (11) to the total absorption of a composite we make the substitution $L \to L^{\rm eff}$, i.e., $A = A_1(L \to L^{\rm eff})$. Equation (11) is the main result of this work. It can be used to calculate the linear and nonlinear absorption. We now elaborate on these two cases.

III. LINEAR ABSORPTION

In the low-fluence limit we set the valence-band occupation to one (completely filled) and the conduction band occupation to zero (completely empty). Equation (11) can be then written as

$$A_1^\pm(T) = \frac{e^2}{\hbar c}\frac{\hbar vL}{S}\frac{\Delta}{4E_\omega}\int_{-\infty}^{\infty} d\varepsilon\left(\frac{1}{E_\omega^2} + \frac{1}{\varepsilon^2+\Delta^2/4}\right) \times \frac{1}{1+\exp\left(\frac{\varepsilon^2+\Delta^2/4-E_\omega^2}{2E_\omega T} \pm \frac{\mu}{T}\right)}. \tag{15}$$

In the intrinsic semiconductor limit ($\mu = 0$) both terms $A_1^\pm$ are the same. In the limit of $T = 0$ Eq. (15) takes the form

$$A_1^\pm(0) = \frac{e^2}{\hbar c}\frac{\hbar vL}{S}\frac{\Delta}{2E_\omega}\left[\frac{\sqrt{E_\omega^2 \pm 2\mu E_\omega - \Delta^2/4}}{E_\omega^2} + \frac{2}{\Delta}\arctan\left(\frac{\sqrt{E_\omega^2 \pm 2\mu E_\omega - \Delta^2/4}}{\Delta/2}\right)\right]. \tag{16}$$

Equation (16) is applicable only when the square roots are real; the corresponding terms should be set to zero otherwise. Physically, vanishing absorption corresponds to the Pauli blocking depicted in Fig. 2(a).

The total linear absorption of a composite can be obtained by making the substitution $L \to L^{\rm eff}$ and is shown in Fig. 2(b)

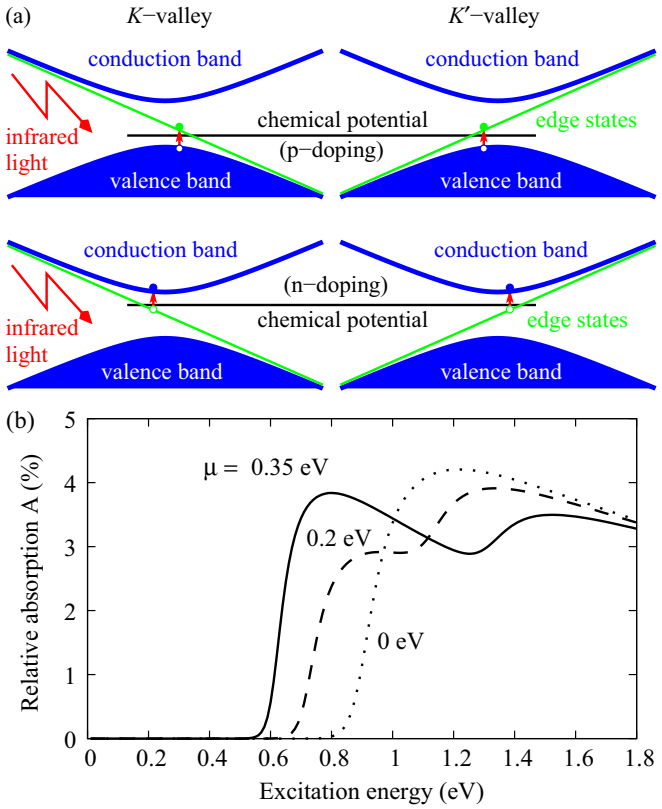

FIG. 2. (a) The possible direct optical transitions at a given radiation wavelength in doped samples. Since the bands are symmetric there is no difference, whether the flakes are n or p doped. (b) Relative linear optical absorption of a MoS_2 dispersion at room temperature computed from Eq. (15). The average flake size $d = 90$ nm and the monolayer flake concentration $n_{2D} = 5.64 \times 10^{11}$ cm^{-2} have been deduced from Refs. [15,16] The band gap $\Delta = 1.8$ eV and the band parameter $\hbar v = 1.1\text{eV} \times 3.193$ Å are taken from Refs. [32,40]. The excitonic and direct valence-to-conduction interband transitions relevant at the excitation energies near Δ are not taken into account. The flakes are n doped with the chemical potential ranging from 0 to 0.35 eV. The spin-orbit splitting is neglected.

as a function of the excitation energy. To be specific, we consider the n-doped samples ($\mu > 0$). The opposite case of $\mu < 0$ results in the same behavior since the bands are assumed to be symmetric with respect to $E = 0$ (the middle of the band gap). At too low excitation energies (when $E_\omega^2 + 2\mu E_\omega - \Delta^2/4 < 0$) the absorption vanishes. Increasing the excitation energy, we first activate the transitions from the edge states to the conduction band. This results in the relative absorption of about 4% for the s-TMD composite we consider. The absorption decreases slightly with the excitation wavelength until the transitions from the valence band to the edge states become activated at $E_\omega^2 - 2\mu E_\omega - \Delta^2/4 > 0$. The dependence $A(E_\omega)$ is therefore nonmonotonic due to the different absorption channels opened at different E_ω. Note that the bands in real MX_2 samples are spin split; therefore, we expect each of two maxima in $A(E_\omega)$ to split into two, which results in a somewhat more complicated pattern. At low doping ($\mu \to 0$) the two maxima merge into a single absorption maximum that can also be seen in Fig. 2.

In order to estimate the absorption maximum by the order of magnitude we consider Eq. (15) in the limit $\mu = 0$ and $T = 0$. The function has a maximum at $E_\omega = 0.67\,\Delta$. At this excitation energy the total linear absorption of a composite film can be estimated as

$$A \sim \frac{4e^2}{\hbar c}\frac{\hbar v}{\Delta}\ell, \tag{17}$$

where ℓ is defined in Eq. (14). The physical meaning is clear: the absorption is larger for smaller Δ because the real-space width of the edge state (5) is larger for smaller gaps. The absorption is proportional to the total length of edges ℓ (per unit square) involved in the absorption. Substituting parameters relevant for MoS_2 [40], and using $d \approx 100$ nm and $n_{2D} \approx 5 \times 10^{11}$ cm^{-2} [15,16], we obtain the subgap absorption of the order of 1%.

IV. SATURABLE ABSORPTION

If the incident fluence Φ is close to the saturation fluence, then the quasi Fermi energies μ_n and μ_p should be taken into account. They can be calculated using the particle conservation. On the one hand, the photocarrier concentration in the conduction band due to the single-edge absorption is $n^{\text{ph}} = \Phi A_1^-/E_\omega$, where A_1^- is the edge-to-conduction-band absorption; see Eq. (11). On the other hand, the same concentration can be calculated for the thermalized electrons as

$$n^{\text{ph}} = \int \frac{d^2k}{4\pi^2}\frac{1}{1+\exp\left(\frac{\sqrt{(\hbar vk)^2+\Delta^2/4}-\mu_n}{T_0}\right)} \approx \frac{T_0\Delta}{4\pi\hbar^2v^2}e^{\frac{\mu_n-\Delta/2}{T_0}}. \tag{18}$$

This approximation is valid as long as $(\Delta/2 - \mu_n)/T_0 \gg 1$. Thus, μ_n can be determined from

$$e^{\frac{\mu_n}{T_0}} = \frac{4\pi\hbar^2v^2}{T_0\Delta}\frac{\Phi A_1^-}{E_\omega}e^{\frac{\Delta}{2T_0}}. \tag{19}$$

The quasi Fermi energy for the valence band μ_p is calculated in the same way using the photoexcited hole concentration $p^{\text{ph}} = \Phi A_1^+/E_\omega$ and its thermalized version, which reads

$$p^{\text{ph}} = \int \frac{d^2k}{4\pi^2}\left(1 - \frac{1}{1+\exp\left(\frac{-\sqrt{(\hbar vk)^2+\Delta^2/4}-\mu_p}{T_0}\right)}\right) \approx \frac{T_0\Delta}{4\pi\hbar^2v^2}e^{-\frac{\mu_p+\Delta/2}{T_0}}. \tag{20}$$

Note that $\mu_p < 0$. Hence, μ_p can be found from

$$e^{-\frac{\mu_p}{T_0}} = \frac{4\pi\hbar^2v^2}{T_0\Delta}\frac{\Phi A_1^+}{E_\omega}e^{\frac{\Delta}{2T_0}}. \tag{21}$$

Now, we employ Eqs. (12) and (13) assuming that

$$\frac{1}{1+\exp\left(-\frac{\varepsilon^2+\Delta^2/4+E_\omega^2}{2E_\omega T_0}-\frac{\mu_p}{T_0}\right)} \approx 1 - \exp\left(-\frac{\varepsilon^2+\Delta^2/4+E_\omega^2}{2E_\omega T_0}-\frac{\mu_p}{T_0}\right),$$

$$\frac{1}{1+\exp\left(\frac{\varepsilon^2+\Delta^2/4+E_\omega^2}{2E_\omega T_0}-\frac{\mu_n}{T_0}\right)} \approx \exp\left(-\frac{\varepsilon^2+\Delta^2/4+E_\omega^2}{2E_\omega T_0}+\frac{\mu_n}{T_0}\right),$$

and exclude $\mu_{n,p}$ using Eqs. (19) and (21). These approximations are standard for semiconductors: we substitute the electron and hole Fermi-Dirac occupations by the corresponding Boltzmann distributions. Note that the edge states are in the metallic regime and therefore the Fermi-Dirac distribution must be retained for this subsystem. To take the integral over ε, we calculate the following expressions:

$$\int_{-\infty}^{\infty}\frac{d\varepsilon}{E_\omega^2}\exp\left(-\frac{\varepsilon^2+\Delta^2/4+E_\omega^2}{2E_\omega T_0}+\frac{\Delta}{2T_0}\right) = \frac{1}{E_\omega}\sqrt{\frac{2\pi T_0}{E_\omega}}\exp\left[-\frac{(E_\omega-\Delta/2)^2}{2E_\omega T_0}\right],$$

$$\int_{-\infty}^{\infty}\frac{d\varepsilon}{\varepsilon^2+\Delta^2/4}\exp\left(-\frac{\varepsilon^2+\Delta^2/4+E_\omega^2}{2E_\omega T_0}+\frac{\Delta}{2T_0}\right) = \frac{2\pi}{\Delta}\exp\left(\frac{\Delta-E_\omega}{2T_0}\right)\mathrm{Erfc}\left(\frac{\Delta}{\sqrt{8E_\omega T_0}}\right),$$

where Erfc is the complementary error function. After some algebra we obtain the saturable absorption in the form

$$A_1^\Phi = \frac{A_1(T)}{1+\frac{\Phi}{\Phi_1^s}}, \tag{22}$$

where $A_1(T)=A_1^+ + A_1^-$ is the linear absorption with $A_1^\pm$ given by Eq. (15). The saturation fluence Φ_1^s can be found from

$$\frac{1}{\Phi_1^s} = \frac{\pi e^2}{\hbar c}\frac{\hbar^3 v^3 L}{E_\omega^3 T_0 S}\exp\left[-\frac{(E_\omega-\Delta/2)^2}{2E_\omega T_0}\right] \times\left[\sqrt{\frac{2\pi T_0}{E_\omega}}+\frac{2\pi E_\omega}{\Delta}e^{\frac{\Delta^2}{8E_\omega T_0}}\mathrm{Erfc}\left(\frac{\Delta}{\sqrt{8E_\omega T_0}}\right)\right]. \tag{23}$$

If we neglect the heating of the edge-state electrons, then we can set $T=T_0$ in Eq. (15), and $A_1^\pm(T)$ can be approximated by $A_1^\pm(0)$ given by Eq. (16). The nonlinear absorption A_1^Φ will be then determined solely by the $(1+\Phi/\Phi_1^s)^{-1}$ multiplier, as if it is the standard two-band model [34]. In order to find the total composite absorption we make the substitution $L\to L^{\mathrm{eff}}$ in Eq. (22) and obtain our main result Eq. (1) with $\Phi^s=\Phi_1^s(L\to L^{\mathrm{eff}})$ and $A=A_1(L\to L^{\mathrm{eff}})$.

We show the composite nonlinear absorption A^Φ in Fig. 3 at the telecommunication wavelength of 1550 nm ($E_\omega=0.8$ eV). The incident fluence can be translated to the intensity as $I=\Phi/\tau$ with τ being the electron-hole recombination time of about 10 ps; see Ref. [41]. The saturation fluence evaluated from Eq. (23) in the excitation energy range 0.8–1.0 eV is of the order of 10 μJ/cm^2 that corresponds to the intensity of the order of 10^6 J/(s cm^2), relevant for the typical measurements [11]. Equation (23) also suggests that the saturation intensity increases dramatically at the excitation energies far from $\Delta/2$. Physically, the half of the band gap $\Delta/2$ plays the same role in our approach as the true band gap Δ in the conventional two-band model [34]. The saturation is most efficient when

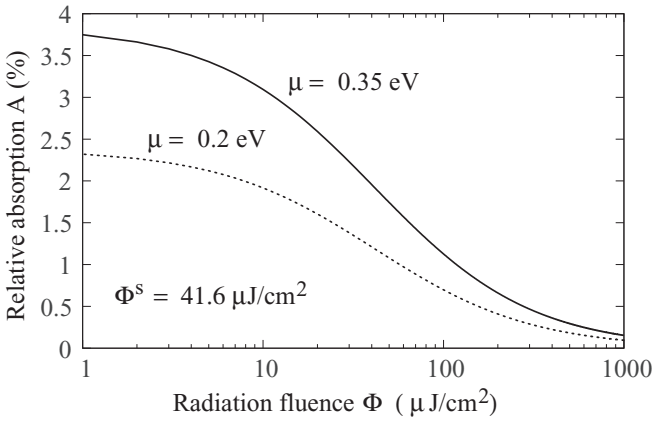

FIG. 3. Saturable optical absorption of a MoS_2 composite at $E_\omega=0.8$ eV. The parameters are the same as in Fig. 2. The saturation fluence is estimated from Eq. (23) with $L\to L^{\mathrm{eff}}$, but Eq. (24) gives nearly the same result for Φ^s of about 40 μJ/cm^2. It corresponds to the intensity of a few MW/cm^2 at the electron-hole recombination time of the order of 10 ps; see Ref. [41].

the photocarriers are excited from and to the band edges. Our model is entering into this regime when the excitation energy is near $\Delta/2$, as one can see from Fig. 1. At the excitation energies much higher than $\Delta/2$, the photocarriers are excited far from the conduction- and valence-band edges and cannot be described by a thermalized distributions (19) and (21). It is instructive to consider the limit $E_\omega=\Delta/2$ and subsequently assume that $\Delta\gg T_0$. The second term in Eq. (23) can be then approximated as $\pi e^{\frac{\Delta}{4T_0}}\mathrm{Erfc}(\sqrt{\frac{\Delta}{4T_0}})\approx\sqrt{\frac{4\pi T_0}{\Delta}}$, and the final formula for the composite saturation fluence reads

$$\frac{1}{\Phi^s}\sim\frac{4\pi^{\frac{3}{2}}e^2}{\hbar c}\frac{\hbar^3 v^3 \ell}{E_\omega^3\sqrt{\Delta T_0}}, \tag{24}$$

where $E_\omega\sim\Delta/2$. The absorption is therefore easier to saturate at smaller gap Δ and longer effective edge length defined in Eq. (14).

V. HOT ELECTRONS ON EDGES

The situation becomes more complicated at the excitation energies higher than half the band gap ($E_\omega>\Delta/2$) in the intrinsic semiconductor regime ($\mu=0$). The energy necessary to promote one edge-state electron to the conduction band (or an edge-state hole to the valence band) is $\Delta/2$. The question we address in this section is what happens with the excess energy $E_\omega-\Delta/2$ after each excitation event.

As already shown in Fig. 1(c), two independent excitation channels corresponding to the valence-to-edge and edge-to-conduction-band transitions are opened. The valence-to-edge-state transitions promote electrons to just above the Fermi level at the same rate as the edge-to-conduction-state transitions create holes just below the Fermi energy; see Fig. 1(c). Effectively, these transitions lift an electron from an edge state below μ to another edge state above μ. If the radiation intensity is high enough (the excitation is faster than the interband recombination), then this results in the generation of electron-hole pairs *within the edge-state subsystem*. Since

electron-electron collisions are very efficient in a one-dimensional case the edge-state electron occupation quickly thermalizes to a Fermi-Dirac distribution with an elevated temperature. Thus, the excess energy is accumulated by the edge-state electrons. Let us quantify this mechanism.

To calculate this temperature, we have to solve the energy balance equation with respect to T:

$$\delta E + E_n + E_p = A_1 S\Phi. \tag{25}$$

The right-hand side of Eq. (25) is the absorbed energy which is balanced with the energies δE, E_n, and E_p accumulated by the thermalized edge, conduction-, and valence-band electrons. The last two can be estimated as $E_n \approx A_1^- S\Phi\Delta/2E_\omega$ and $E_p \approx A_1^+ S\Phi\Delta/2E_\omega$, where the same approximation as in Eqs. (18) and (20) has been utilized. Physically, E_n (E_p) is the product between the photoexcited electron (hole) number $A_1^\mp \Phi S/E_\omega$ and the typical energy $\pm\Delta/2$ in thermalized limit. The energy pumped into the edge-state electron gas can be calculated assuming that the occupation is already thermalized and given by the Fermi-Dirac distribution function. The edge-state electron-hole excitation energy is the difference between the electron and hole energies within the edge-state band, as shown in Fig. 1(c) by dashed lines. It can be written as

$$\begin{aligned} E(T) &= \int_{-\infty}^{-\frac{\mu}{\hbar v}} \frac{dk_x L}{2\pi} \frac{-\hbar v k_x}{1+\exp\left(\frac{-\hbar v k_x-\mu}{T}\right)} \\ &\quad - \int_{-\frac{\mu}{\hbar v}}^{\infty} \frac{dk_x L}{2\pi} \frac{-\hbar v k_x}{1+\exp\left(\frac{\hbar v k_x+\mu}{T}\right)} \\ &= \frac{\pi T^2 L}{12\hbar v}. \end{aligned} \tag{26}$$

Note that $E(T)$ does not depend on μ because of the linear dispersion, hence δE is independent of μ as well and reads

$$\delta E = \frac{\pi L}{12\hbar v}\left(T^2 - T_0^2\right). \tag{27}$$

Equation (25) is then written as

$$\frac{\pi\left(T^2 - T_0^2\right)}{12\hbar v}\frac{L}{S} = \left(1 - \frac{\Delta}{2E_\omega}\right)\Phi A_1. \tag{28}$$

Substituting $L \to L^{\text{eff}}$, $A_1 \to A^\Phi$ we obtain the following equation for the edge-state electron temperature in a composite:

$$\begin{aligned} T^2 - T_0^2 &= \frac{3\hbar e^2 v^2 \Phi\Delta}{\pi c E_\omega} \frac{1-\Delta/(2E_\omega)}{1+\Phi/\Phi^s} \\ &\quad \times \sum_{\pm} \int_{-\infty}^{\infty} d\varepsilon \frac{(E_\omega)^{-2} + (\varepsilon^2+\Delta^2/4)^{-1}}{1+\exp\left(\frac{\varepsilon^2+\Delta^2/4-E_\omega^2}{2E_\omega T} \pm \frac{\mu}{T}\right)}. \end{aligned} \tag{29}$$

This equation can be solved with respect to T numerically using the method of iterations (the method of consecutive approximations). The result is demonstrated in Fig. 4, where absorption and edge-state carrier temperature are shown for different excitation energies. If $E_\omega = \Delta/2$, then the solid and dashed curves coincide, and heating of the edge-state electrons (solid curve) can be neglected. If $E_\omega > \Delta/2$, then the excess energy $E_\omega - \Delta/2$ is pumped into the edge-state electron subsystem and its temperature can reach 0.1 eV (~1200 K). The high temperature makes the edge states evenly populated in k_x space that results in less electrons excited from the edge states to the conduction band and less empty space available for the electrons coming from the valence band. Hence, the elevated temperature slightly reduces absorption, as shown in Fig. 4.

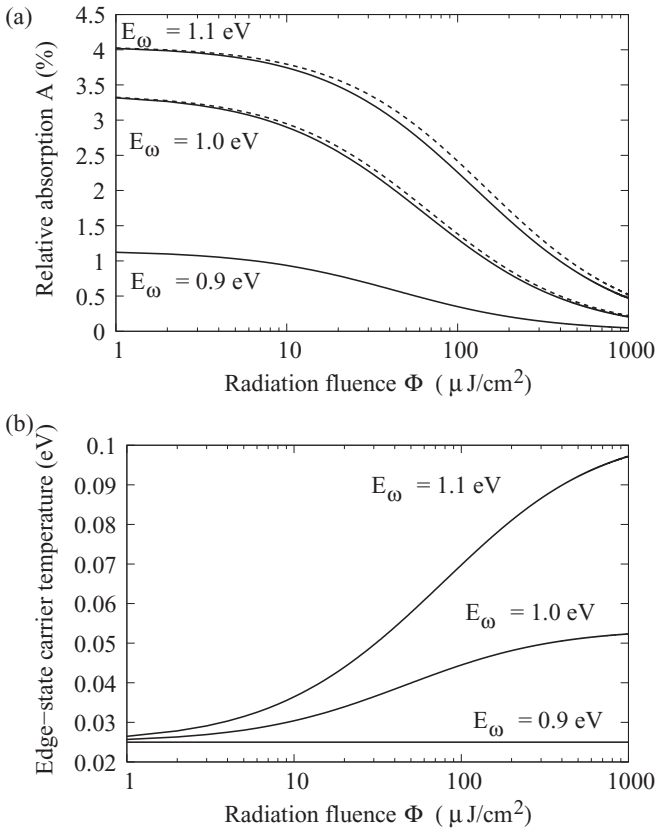

FIG. 4. (a) Saturable absorption in the intrinsic limit ($\mu = 0$) at different excitation energies $E_\omega \geqslant \Delta/2$. The dashed curves correspond to the simplified model where the edge-state electron temperature remains constant. The solid curves take into account the energy pumping due to the processes shown in Fig. 1(b). At the excitation energies higher than $\Delta/2$, the deviation between the solid and dashed curves is clearly visible. (b) Edge-state electron temperature vs fluence computed from Eq. (29).

VI. CONCLUSION AND OUTLOOK

In conclusion, we have developed a simple model to qualitatively describe edge-state mediated absorption in s-TMD flakes and s-TMD-polymer composites. We show that the appropriate description must involve a three-level system, in contrast to the conventional two-band model routinely used for semiconductors [34]. At excitation energies near $\Delta/2$, the linear absorption of a s-TMD composite can be estimated using Eq. (17), while the saturation fluence is given by Eq. (24). The band structure parameters in Eqs. (17) and (24) can be calculated [32,42] or measured [40]. Our estimates of linear and saturable absorption agree, to within one order of magnitude, with existing saturable absorption measurements performed on WS_2 [9] and $MoSe_2$ [11,12] composites. We stress that this work does not aim at a quantitative analysis of specific samples. For this, the following should be considered.

(1) Due to the spin-orbit splitting in the valence band, the band gap is different for each spin channel. Strictly speaking, we have *four* terms in the absorption, $A^{+}_{\uparrow}$, $A^{-}_{\uparrow}$, $A^{+}_{\downarrow}$, and $A^{-}_{\downarrow}$, instead of two $A^{\pm}$ considered here. The nonmonotonic dependence of the linear absorption on the excitation energy shown in Fig. 2 becomes more complicated once we take into account the spin splitting.

(2) The light beam is assumed to be normal to the flakes. The plane of incidence is therefore not well defined; consequently, our model is insensitive to s and p polarization. This is not the case in real MX_2 composites where flakes are randomly oriented within the host polymer matrix. The quantitative model should therefore include averaging not only over the azimuthal polarization angle θ_E performed here but also over the polar angle, as described in Ref. [43].

(3) The majority of the experimental examples of s-TMDs for ultrafast photonics exploit ultrasonic or shear assisted LPE of their bulk crystals [44]. Such dispersions and composites mostly contain few-layer crystals [7,11,16]. In our model, we assume that the interlayer coupling is weak for the flakes produced by LPE, and any thin N-layer flake can be viewed as a stack of N monolayers, without such coupling. This approach works well for graphene [45], but a quantitative model for s-TMDs should address this more carefully.

(4) Our formula for saturation fluence Eq. (23) is not reliable for excitation energies far from $\Delta/2$. This is because at such energies the photocarriers are excited far from the band edges and cannot be described by a thermalized distribution used here. In order to improve the reliability of the model a nonthermalized distribution for conduction- and valence-band photocarriers should be employed.

(5) To calculate the hot electron temperature, we assume that there is no energy dissipation at the time scale of the incident pump pulse duration or the electron-hole recombination process, whichever is shorter. A quantitative model should include an additional term in the energy balance equation (25) to take into account energy relaxation.

(6) The model neglects defects in crystals completely. These defects could result in an additional nonsaturable term in Eq. (1) for the nonlinear absorption A^{Φ}.

As an outlook we propose the following experiment to verify our model. Our theory predicts that the edge-state optical absorption increases with the ratio of the total edge length to area of the composite film. The crystallographic faults, impurities, and other bulk defects cannot result in such behavior. Thus, reducing the size of flakes but keeping their mass concentration constant we can increase the edge-state contribution to the total absorption and hence distinguish between the edge and bulk effects.

In addition to MX_2 flakes, our model could be applied to other hexagonal nanostructured composites, e.g., boron nitride (h-BN) monolayers, where the band-gap size $\Delta = 3.92$ eV and the band-gap parameter $\hbar v = 2.33\,\text{eV} \times 2.174\,\text{Å}$ [46]. This results in lower edge-state absorption, but the optimum excitation energy $E_\omega \approx \Delta/2$ lies in the visible region, near the wavelength of 630 nm, suggesting h-BN may also be a suitable platform for the design of nonlinear composite-based devices in the visible spectral range.

ACKNOWLEDGMENTS

The authors thank R. I. Woodward, R. C. T. Howe, G. Hu, and W. Belzig for fruitful discussions. E.J.R.K. and T.H. acknowledge funding support from the Royal Academy of Engineering (United Kingdom). M.T. thanks Collaborative Research Center 767 for support.

[1] A. K. Geim, Rev. Mod. Phys. **83**, 851 (2011).
[2] M. Xu, T. Liang, M. Shi, and H. Chen, Chem. Rev. **113**, 3766 (2013).
[3] Q. H. Wang, K. Kalantar-Zadeh, A. Kis, J. N. Coleman, and M. S. Strano, Nature Nanotechnology **7**, 699 (2012).
[4] K. F. Mak, C. Lee, J. Hone, J. Shan, and T. F. Heinz, Phys. Rev. Lett. **105**, 136805 (2010).
[5] T. Korn, S. Heydrich, M. Hirmer, J. Schmutzler, and C. Schüller, Appl. Phys. Lett. **99**, 102109 (2011).
[6] A. Splendiani, L. Sun, Y. Zhang, T. Li, J. Kim, C.-Y. Chim, G. Galli, and F. Wang, Nano Lett. **10**, 1271 (2010).
[7] M. Zhang, R. Howe, R. I. Woodward, E. J. Kelleher, F. Torrisi, G. Hu, S. Popov, J. Taylor, and T. Hasan, Nano Research **8**, 1522 (2015).
[8] R. I. Woodward, E. Kelleher, R. Howe, G. Hu, F. Torrisi, T. Hasan, S. Popov, and J. Taylor, Opt. Express **22**, 31113 (2014).
[9] M. Zhang, G. Hu, G. Hu, R. Howe, L. Chen, Z. Zheng, and T. Hasan, Scientific Reports **5**, 17482 (2015).
[10] D. Mao, Y. Wang, C. Ma, L. Han, B. Jiang, X. Gan, S. Hua, W. Zhang, T. Mei, and J. Zhao, Scientific Reports **5**, 7965 (2015).
[11] R. I. Woodward, R. C. T. Howe, T. H. Runcorn, G. Hu, F. Torrisi, E. J. R. Kelleher, and T. Hasan, Opt. Express **23**, 20051 (2015).
[12] Z. Luo, Y. Li, M. Zhong, Y. Huang, X. Wan, J. Peng, and J. Weng, Photonics Research **3**, A79 (2015).
[13] Y. Zhang, T.-R. Chang, B. Zhou, Y.-T. Cui, H. Yan, Z. Liu, F. Schmitt, J. Lee, R. Moore, Y. Chen *et al.*, Nature Nanotechnology **9**, 111 (2014).
[14] S. Wang, H. Yu, H. Zhang, A. Wang, M. Zhao, Y. Chen, L. Mei, and J. Wang, Adv. Mater. **26**, 3538 (2014).
[15] R. I. Woodward, R. C. T. Howe, G. Hu, F. Torrisi, M. Zhang, T. Hasan, and E. J. R. Kelleher, Photon. Res. **3**, A30 (2015).
[16] R. C. T. Howe, R. I. Woodward, G. Hu, Z. Yang, E. J. R. Kelleher, and T. Hasan, Phys. Status Solidi B **253**, 911 (2016).
[17] C. Roxlo, R. Chianelli, H. Deckman, A. Ruppert, and P. Wong, J. Vac. Sci. Technol. A **5**, 555 (1987).
[18] C. G. Péterfalvi, A. Kormányos, and G. Burkard, Phys. Rev. B **92**, 245443 (2015).
[19] L. Brey and H. A. Fertig, Phys. Rev. B **73**, 235411 (2006).
[20] A. R. Akhmerov and C. W. J. Beenakker, Phys. Rev. B **77**, 085423 (2008).
[21] J. Lado, N. Garcia-Martinez, and J. Fernandez-Rossier, Synth. Met. **210**, 56 (2015).
[22] S. Pavlović and F. M. Peeters, Phys. Rev. B **91**, 155410 (2015).
[23] C. Segarra, J. Planelles, and S. E. Ulloa, Phys. Rev. B **93**, 085312 (2016).

[24] M. V. Bollinger, J. V. Lauritsen, K. W. Jacobsen, J. K. Nørskov, S. Helveg, and F. Besenbacher, Phys. Rev. Lett. **87**, 196803 (2001).
[25] M. V. Bollinger, K. W. Jacobsen, and J. K. Norskov, Phys. Rev. B **67**, 085410 (2003).
[26] Y. Li, Z. Zhou, S. Zhang, and Z. Chen, J. Am. Chem. Soc. **130**, 16739 (2008).
[27] A. Vojvodic, B. Hinnemann, and J. K. Nørskov, Phys. Rev. B **80**, 125416 (2009).
[28] L. Kou, C. Tang, Y. Zhang, T. Heine, C. Chen, and T. Frauenheim, J. Phys. Chem. Lett. **3**, 2934 (2012).
[29] E. Erdogan, I. Popov, A. Enyashin, and G. Seifert, Eur. Phys. J. B **85**, 33 (2012).
[30] G. Xu, J. Wang, B. Yan, and X.-L. Qi, Phys. Rev. B **90**, 100505 (2014).
[31] H. Pan and Y.-W. Zhang, J. Mater. Chem. **22**, 7280 (2012).
[32] D. Xiao, G.-B. Liu, W. Feng, X. Xu, and W. Yao, Phys. Rev. Lett. **108**, 196802 (2012).
[33] M. V. Berry and R. J. Mondragon, Proc. R. Soc. A **412**, 53 (1987).
[34] E. Garmire, IEEE J. Sel. Top. Quantum Electron. **6**, 1094 (2000).
[35] E. McCann, *Graphene Nanoelectronics: Metrology, Synthesis, Properties and Applications* (Springer-Verlag, Berlin, 2012), Chap. 8.
[36] M. Z. Hasan and C. L. Kane, Rev. Mod. Phys. **82**, 3045 (2010).
[37] M. Trushin, A. Grupp, G. Soavi, A. Budweg, D. De Fazio, U. Sassi, A. Lombardo, A. C. Ferrari, W. Belzig, A. Leitenstorfer *et al.*, Phys. Rev. B **92**, 165429 (2015).
[38] M. Trushin and J. Schliemann, Europhys. Lett. **96**, 37006 (2011).
[39] J. Nelson, *The Physics of Solar Cells* (Imperial College Press, UK, 2004).
[40] B. S. Kim, J.-W. Rhim, B. Kim, C. Kim, and S. R. Park, arXiv:1601.01418 (2016).
[41] H. Wang, C. Zhang, and F. Rana, Nano Lett. **15**, 8204 (2015).
[42] A. Kormányos, G. Burkard, M. Gmitra, J. Fabian, V. Zólyomi, N. D. Drummond, and V. Fal'ko, 2D Materials **2**, 022001 (2015).
[43] K. R. Paton and J. N. Coleman, arXiv:1511.04410 (2015).
[44] R. C. T. Howe, G. Hu, Z. Yang, and T. Hasan, Proc. SPIE **9553**, 95530R (2015).
[45] Z. Sun, T. Hasan, F. Torrisi, D. Popa, G. Privitera, F. Wang, F. Bonaccorso, D. M. Basko, and A. C. Ferrari, ACS Nano **4**, 803 (2010).
[46] R. M. Ribeiro and N. M. R. Peres, Phys. Rev. B **83**, 235312 (2011).